Rayleigh-Bénard Convection in a Vertically Oscillated Fluid Layer

Jeffrey L. Rogers† and Michael F. Schatz*
School of Physics, Georgia Institute of Technology, Atlanta, Georgia 30332-0430

Jonathan L. Bougie and Jack B. Swift
Department of Physics and Center for Nonlinear Dynamics, University of Texas, Austin, Texas 78712
(Received 2 July 1999)

We report on the first quantitative observations of convection in a fluid layer driven by both heating from below and vertical sinusoidal oscillation. Just above onset, convection patterns are modulated either harmonically or subharmonically to the drive frequency. Single-frequency patterns exhibit nearly solid-body rotations with harmonic and subharmonic states always rotating in opposite directions. Flows with both harmonic and subharmonic responses are found near a codimension-two point, yielding novel coexisting patterns with symmetries not found in either single-frequency states. Predictions from linear stability analysis of the onset Rayleigh and wave numbers compare well with experiment, and phase boundaries for coexisting patterns track single-frequency marginal stability curves.

PACS numbers: 47.54.+r, 47.20.Bp, 47.20.Lz

Characterizing pattern formation is a fundamental problem in the study of nonequilibrium systems. Wave number selection mechanisms provide one useful means for identifying common pattern forming behaviors in diverse physical systems [1]. The pattern wave number q may be selected by geometrical constraints; a canonical example of *geometry-induced* patterns is found in Rayleigh-Bénard convection where the pattern length scale is governed by the fluid layer thickness d [2]. By contrast, the selected q may depend on an externally imposed frequency ω in systems subjected to spatially uniform, time-periodic oscillation [1]; a common example of these *dispersion-induced* patterns is the parametric excitation of surface waves (Faraday waves) in an open container of fluid [2]. Pattern selection by these generic mechanisms also arises in nonhydrodynamic systems; geometry-induced patterns occur in the buckling instability of thin plates [3], while dispersion-induced patterns are generated by optical waves in a fiber laser [4] and crystallization waves in ^{4}He [5].

We report the first experimental observations of both geometry-induced (onset q weakly dependent on ω) and dispersion-induced (onset q strongly dependent on ω) patterns in a single system: a fluid layer that is both heated from below and vertically oscillated sinusoidally. Fluid motion in this system requires a thermally induced density variation, as characterized by the Rayleigh number R (Fig. 1). When the drive amplitude δ or oscillation frequency ω are small, we observe fluid motion modulated at ω [harmonic (H)] and geometry-induced spatial structure [Fig. 1(a)] reminiscent of standard Rayleigh-Bénard convection [6]. For sufficiently large δ or ω, flows arise with modulation at $\omega/2$ [subharmonic (S)], characteristic of dispersion-induced Faraday wave patterns. Our measurements for the onset of these patterns quantitatively test both stability calculations and numerical simulations performed over the past thirty years [7–12]. Patterns exhibit nearly solid-body rotation over a wide parameter range with H and S patterns always rotating in opposite directions. In addition, we find and characterize a region of parameter space where the distinct spatial and temporal scales of H and S patterns interweave to form complex states [Figs. 1(e) and 1(f)], including localized domains of one pattern embedded in the other, mode-locking, and formation of pattern symmetries not found in either pure state.

Experiments are performed on a layer of CO_2 gas bounded below by a 0.6-cm-thick gold-coated aluminum mirror, laterally by a 3.80 ± 0.03 cm inner diameter ring of filter paper, and above by a 2.54-cm-thick sapphire window. Two cell depths are studied: $d = (6.50 \text{ and } 6.72 \pm 0.03) \times 10^{-2}$ cm, corresponding to a vertical diffusion time of $\tau_v \equiv d^2/\kappa \approx 2$ s. Length is scaled by d and time by τ_v. Thermal gradients are imposed across the fluid layer by heating the mirror from below and using circulating water to cool the window from above resulting in a vertical temperature difference (ΔT) controlled to within ± 0.01 °C. The fluid layer is vertically vibrated sinusoidally by a hydraulic piston under closed-loop control rendering oscillations with less than 4% of the total amplitude in higher harmonics. Patterns are visualized using shadowgraphy and recorded by a digital image acquisition system. To determine H or S amplitude modulation pattern images are captured at ~20 Hz (twice the drive frequency) while long-time dynamics are recorded at ~0.5 Hz using a shutter synchronized with the piston motion. For $\delta = 0$ (no oscillations), the conductive state loses stability to roll patterns, suggesting that non-Boussinesq effects are weak and occur below the limit of our temperature resolution. These observations are consistent with our calculations using a variational model described by previous authors [13–15], which demonstrate rolls are the globally stable state for R only ~0.3% larger than the unmodulated critical value, $R_c^0 = 1708$. Patterns are explored with

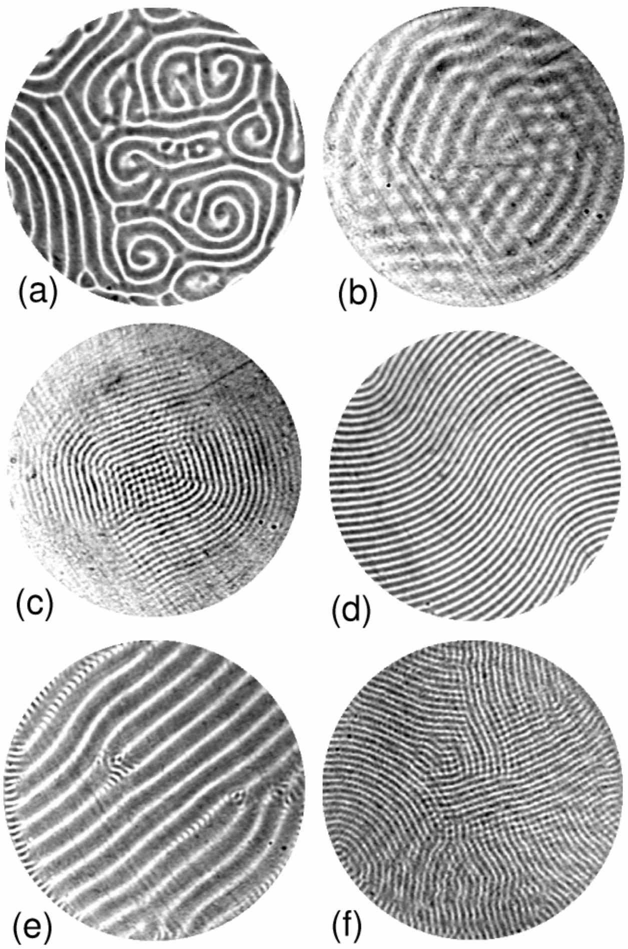

FIG. 1. Convection patterns are visualized using shadowgraphy and characterized by four dimensionless quantities: Prandtl number $\mathrm{Pr} = \frac{\nu}{\kappa} = 0.93$, driving frequency $\omega = \frac{d^2}{\kappa} 2\pi f = 98$, displacement amplitude $\delta = \frac{\kappa^2}{g d^4}\delta'$, and Rayleigh number $R = \frac{\alpha g d^3 \Delta T}{\nu\kappa}$, while the kinematic viscosity ν, thermal diffusivity κ, thermal expansion coefficient α, forcing frequency f (Hz), amplitude δ' (cm), and gravitational acceleration $g = 980$ ($\frac{\mathrm{cm}}{\mathrm{s}^2}$). (a) H spiral defect chaos ($\delta = 1.76 \times 10^{-4}, R = 3198$). (b) Coexisting H rolls and hexagons ($\delta = 3.74 \times 10^{-4}, R = 4216$). (c) S rolls near onset ($\delta = 4.26 \times 10^{-4}, R = 3958$). (d) S rolls ($\delta = 4.05 \times 10^{-4}, R = 4990$). (e) H rolls with localized domains of S rolls ($\delta = 3.76 \times 10^{-4}, R = 4962$). (f) S rolls containing grain boundaries overlaying a weak pattern of H rolls and cells ($\delta = 3.64 \times 10^{-4}, R = 5424$).

ω and Pr held constant (Fig. 1) while increasing and decreasing δ at various fixed values of R.

H convection occurs for small δ [Fig. 2(a)]. Without oscillations ($\delta = 0$) spiral defect chaos arises for $R \gtrsim 2500$ in agreement with previous experiments [6]. With oscillations ($\delta > 0$ at fixed R), spiral defect chaos modulated at ω persists for a significant range in δ (e.g., $\delta \lesssim 3.30 \times 10^{-4}$ at $R = 4840$). With increasing δ the number of spiral defects decrease as more regular states whose morphology depends on R emerge. For $2500 \lesssim R \lesssim 3900$ these emerging patterns are typically multiarm spirals which reduce in arm number, eventually becoming targets as the conduction state is approached. At larger R ($3900 \lesssim R \lesssim 5500$) spiral defect chaos becomes a pattern of nearly parallel rolls tending to terminate perpendicular to the sidewalls and possessing several foci at the boundaries; the number of foci and curvature of the associated rolls decreases with increasing δ. The transition with increasing δ from spiral defect chaos to parallel rolls is reminiscent of the well-studied transition in unmodulated Rayleigh-Bénard convection for decreasing R [16]. For $3100 \lesssim R < 4560$ uniform parallel rolls or targets lose stability with increasing δ as domains of hexagons form [Fig. 1(b)]. These states of hexagons and rolls or targets occur only for a narrow range ($\approx 6 \times 10^{-6}$) of δ before losing stability to conduction with a small additional increase in δ. Within the experimental resolution in δ ($\approx 2 \times 10^{-6}$) no hysteresis is observed in the transition between the hexagon-roll states and conduction. The nonhysteretic transition and morphology of these patterns are consistent with other modulated Rayleigh-Bénard experiments involving time-periodic driving of the bottom plate temperature [17].

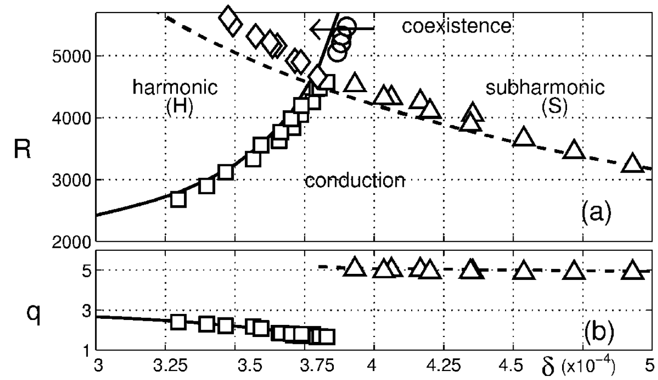

FIG. 2. Phase diagram and comparison of linear stability predictions to experiments at $\omega = 98$. The phase diagram (a) contains regions of conduction, convection with H (ω) and S ($\omega/2$) modulations, as well as coexisting H-S patterns. Marginal stability curves computed for the conduction state subjected to H (solid line) and S (dashed) perturbations agree with the measured values of R_c (a) and q_c (b) at the onset of H ($\square$) and S ($\triangle$) convection. The measured transition to coexisting patterns from pure H ($\diamond$) and S ($\bigcirc$) states is compared to the marginal stability predictions for *conduction*. The maximum displacement ($\delta = 5 \times 10^{-4}$) corresponds to an acceleration of $\sim 5g$.

S convection is observed for sufficiently large δ [Fig. 2(a)]. The onset of S patterns occurs as a uniform patch of rolls; no hysteresis or hexagons are observed, consistent with the S temporal symmetry that excludes three wave interactions [2]. With increasing δ other roll domains form with grain boundaries at the domain intersections. The roll domains merge with further increase in δ, leading to the formation of disclinations that may interact [Fig. 1(c)]. For sufficiently large δ, either a single convex disclination or, less frequently, a spiral arises centered within the convection cell. These patterns experience skew-varicose instabilities leading to repeated

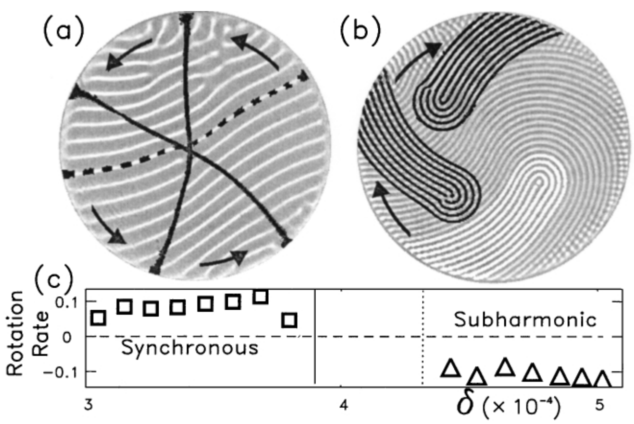

FIG. 3. H (□) and S (△) patterns rotate in opposite directions. (a) At $\delta = 3.47 \times 10^{-4}$ the motion of a single H roll (dashed line) is followed in time at intervals of $11.3\tau_v$. (b) At $\delta = 4.53 \times 10^{-4}$ the motion of a S disclination (bright white region) is followed in time at intervals of $15.0\tau_v$. (c) The dimensionless rotation rate versus δ for $R = 3920$ and $\omega = 98$.

nucleation of dislocations; additionally the patterns may move off center [Fig. 3(b)]. With increasing δ a single roll domain forms with few dislocations and a long wavelength distortion [Fig. 1(d)]. Patterns qualitatively similar to Fig. 1(d) have been previously observed in rotating Rayleigh-Bénard convection [18].

Following the method described by previous investigators [10,11] we performed a linear stability analysis of the conductive state. The resulting predictions for both critical Rayleigh numbers R_c and critical wave numbers q_c are in good agreement with the experimentally observed values at onset of both H and S convection (Fig. 2). For H convection, modulation enhances the stability of conduction ($R_c > R_c^0$) while decreasing q_c below its unmodulated value $q_c^0 = 3.117$, consistent with previous modulated Rayleigh-Bénard experiments [17]. In addition, for S convection $R_c > R_c^0$ and q_c decrease with increasing δ (Fig. 2). For parameter values not studied here R_c is predicted to drop below R_c^0 [10].

For $R \gtrsim 2500$ patterns undergo nearly solid-body rotation where H and S states rotate opposite directions (Fig. 3). For fixed R ($2500 \lesssim R \lesssim 4560$) and increasing δ from zero, the onset of rotation occurs near $\delta \approx 2 \times 10^{-4}$. Patterns deviate somewhat from ideal solid-body rotation because point defects and grain boundaries continually propagate within the rotating patterns. Global rotation rate increases with δ except near the conduction boundaries where rotation slows as patterns weaken [Fig. 3(c)]. A given rotation direction is selected and maintained by the patterns throughout the duration of an experimental trial. Patterns do not equally select clockwise and counterclockwise directions; in 62 separate experiments H states rotated counterclockwise in 84% of the trials. In all cases, H and S patterns rotate in opposite directions. Rotations are qualitatively robust against perturbations from tilting the apparatus $\sim 5°$ off the vertical, changing the sidewalls to square symmetry and asymmetric cooling of the top plate.

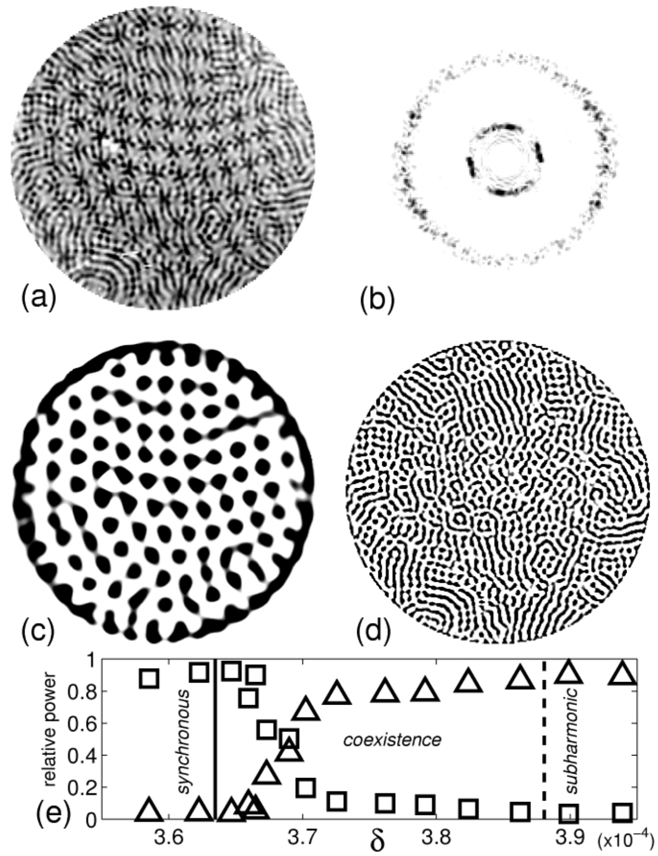

FIG. 4. Coexisting H and S patterns (a) ($\delta = 3.62 \times 10^{-4}$, $\omega = 108$ and $R = 5515$) may be decomposed by filtering in the wave number domain (b) to yield both H (c) and S (d) components; in this case, both components equal power to the wave number spectrum (b) and exhibit mode locking of the wave numbers ($\frac{q_S}{q_H} = \frac{5.02}{1.67} = 3.01$). (e) The relative power contributed by H (□) and S (△) components to wave number spectra changes abruptly as a function of δ for constant $\omega = 98$ and $R = 5320$. Vertical lines mark the measured coexistence boundaries.

For $R > 4560$ conduction is no longer stable; instead H and S patterns compete and coexist over a range of δ between the pure states [Fig. 2(a)]. As δ is increased, pure H states lose stability to mixed patterns where localized patches of S rolls form about H defects and are advected along as the defects propagate. At slightly larger δ [e.g., $\delta = 3.67 \times 10^{-4}$ in Fig. 4(e)], S rolls begin to form perpendicular to H upflows throughout the pattern [Fig. 1(e)]. The wave number of emerging S rolls (q_S) is close to the second harmonic of the H pattern wave number (q_H). A small change in δ [e.g., $\delta = 3.69 \times 10^{-4}$ in Fig. 4(e)] yields states where H patterns of local hexagonal, square, and rhombic symmetries are mixed with rolls of the S component perpendicular to the cell faces [Figs. 4(a), 4(c), and 4(d)]. For these states, the H and S components contribute equal power to the wave number spectra and have mode-locked wave numbers ($\frac{q_S}{q_H} = 3$). With further small increases in δ [$\delta \gtrsim 3.72 \times 10^{-4}$ in Fig. 4(e)], the S component dominates the power spectra and, concurrently, the wave number ratio unlocks ($\frac{q_S}{q_H} < 2.8$) as q_H increases abruptly. The S component forms domains of increasingly larger size as the H component gradually weakens [Fig. 1(f)]. Upon crossing the phase boundary with purely S states [Fig. 2(a)] rolls with a long-wavelength distortion are typically observed [Fig. 1(d)].

The experimentally determined phase boundaries separating coexisting states from the pure patterns track the marginal stability curves for the *conduction* state [Fig. 2(a)]. For $R > 4560$, the H marginal stability curve is in nearly exact agreement with the phase boundary between coexisting and pure S states. This suggests the S base state from which H convection bifurcates differs little from conduction in a spatially averaged sense. Spatial Fourier spectra support this viewpoint since the higher modes of S patterns cannot overlap with the smaller wave number H fundamental. By contrast, the experimentally determined phase boundary between coexisting and pure H states lies above the S marginal stability curve, suggesting that H convection inhibits the onset of S convection due to wave number interaction. Evidence for this inhibitory effect is further bolstered by the observation that S convection first appears near H pattern defects. The amplitude of convective flow is generally suppressed in the cores of pattern defects [19] and, therefore, any inhibitory effect of H convection on S patterns should be weaker near defects. Moreover, a previous stability analysis of the H base state suggests the onset of S convection is delayed by the presence of H convection [10].

These multiple length scale convection patterns differ qualitatively from coexisting wavelength states in spatially separate domains observed in optical systems [20] as well as quasiperiodic [21] and superlattice [22] states reported in Faraday experiments. Three wave interactions (resonant triads) are responsible for multiscale Faraday patterns; it seems doubtful resonant triads are important in the convection patterns described here due to the S temporal symmetry and large difference between q_H and q_S. Resonant triads may be introduced in convection patterns by non-Boussinesq effects and for the current experiment with heating from above squares and quasiperiodic structures have been predicted [12].

This work is supported by the NASA Office of Life and Microgravity Sciences Grants No. NAG3-2006 (at the Georgia Institute of Technology) and No. NAG3-1839 (at the University of Texas-Austin).

†Electronic address: jeff@einstein.physics.gatech.edu
*Electronic address: mike.schatz.physics.gatech.edu

[1] P. Coullet, T. Frisch, and G. Sonnino, Phys. Rev. E **49**, 2087 (1994).
[2] M. C. Cross and P. C. Hohenberg, Rev. Mod. Phys. **65**, 851 (1993).
[3] M. Boucif, J. E. Wesfried, and E. Guyon, Eur. J. Mech. A, Solids **10**, 641 (1991).
[4] C. Szwaj, S. Bielawski, D. Derozier, and T. Erneux, Phys. Rev. Lett. **80**, 3968 (1998).
[5] W. van Saarloos and J. D. Weeks, Phys. Rev. Lett. **74**, 290 (1995).
[6] S. Morris, E. Bodenschatz, G. Ahlers, and D. S. Cannell, Phys. Rev. Lett. **71**, 2026 (1993).
[7] P. M. Grasho and R. L. Sani, J. Fluid Mech. **40**, 783 (1970).
[8] G. Z. Gershuni and D. V. Lyubimov, *Thermal Vibrational Convection* (Wiley, Chichester, 1998).
[9] G. Ahlers, P. C. Hohenberg, and M. Lücke, Phys. Rev. A **32**, 3493 (1985); **32**, 3519 (1985).
[10] R. Clever, G. Schubert, and F. H. Busse, J. Fluid Mech. **253**, 663 (1993).
[11] R. Clever, G. Schubert, and F. H. Busse, Phys. Fluids A **5**, 2430 (1993).
[12] U. E. Volmar and H. W. Müller, Phys. Rev. E **56**, 5423 (1997).
[13] F. H. Busse, J. Fluid Mech. **30**, 625 (1967).
[14] B. A. Malomed, A. A. Nepomnyashchy, and M. I. Tribelshy, Phys. Rev. A **42**, 7244 (1990).
[15] E. Bodenschatz, J. R. de Bruyn, G. Ahlers, and D. S. Cannell, Phys. Rev. Lett. **67**, 3078 (1991).
[16] S. Morris, E. Bodenschatz, D. S. Cannell, and G. Ahlers, Physica (Amsterdam) **97D**, 164 (1996).
[17] C. W. Meyer, D. S. Cannell, and G. Ahlers, Phys. Rev. A **45**, 8583 (1992).
[18] Y. Hu, R. E. Ecke, and G. Ahlers, Phys. Rev. E **55**, 6928 (1997).
[19] M. C. Cross, Phys. Rev. A **25**, 1065 (1982).
[20] E. Pampaloni, S. Residori, S. Soria, and F. T. Arecchi, Phys. Rev. Lett. **78**, 1042 (1997), and references therein.
[21] W. S. Edwards and S. Fauve, J. Fluid Mech. **278**, 123 (1994).
[22] C. Wagner, H. W. Müller, and K. Knorr, Phys. Rev. Lett. **83**, 308 (1999); H. Arbell and J. Fineberg, Phys. Rev. Lett. **81**, 4384 (1998); A. Kudrolli, B. Pier, and J. P. Gollub, Physica (Amsterdam) **123D**, 99 (1998).